Convective Patterns in Binary Fluid Mixtures with Positive Separation Ratios

Björn Huke and Manfred Lücke

Institut für Theoretische Physik, Universität des Saarlandes, Postfach 151150, D-66041 Saarbrücken, Germany

Abstract. We summarize our findings about laterally periodic convection structures in binary mixtures in the Rayleigh–Bénard system for positive Soret effect. Stationary roll, square, and crossroll solutions and their stability are determined with a multimode Galerkin expansion. The oscillatory competition of squares and rolls in the form of crossroll oscillations is reviewed. They undergo a subharmonic bifurcation cascade where the oscillation period grows in integer steps as a consequence of an entrainment process.

1 Introduction

The Rayleigh–Bénard system is a prominent example for studying pattern formation in hydrodynamic systems driven away from equilibrium. In this system a fluid layer is confined between two extended plates perpendicular to the direction of gravity. A temperature difference between lower and upper plate is applied. Below a critical temperature difference a quiescent conductive state is established wherein the temperature varies linearly between the plates. But for larger differences buoyancy forces are strong enough to destabilize this conductive state and to start convection.

The pure fluid convection in the Rayleigh–Bénard system at moderate heating rates is experimentally and theoretically well investigated [1]. An extension of the problem that leads to more complex convection behavior is achieved by using binary mixtures such as ethanol-water instead. In binary mixtures the buoyancy forces are also influenced by concentration variations. The structural dynamics of the concentration distribution in mixtures results from an interplay between three competing mechanisms: nonlinear advection and mixing, weak solutal diffusion, and the Soret effect. The latter generates and sustains concentration gradients in linear response to local temperature gradients. Without Soret coupling measured by the separation ratio any concentration fluctuation diffuses away.

Convection in binary mixtures shows a rich spectrum of pattern formation behavior [1–3]. But the knowledge about these structures and in particular about their stability is more limited than for pure fluids. This is especially true for the case of a positive Soret effect where the fact that the novel structures are three-dimensional makes their numerical investigation more difficult.

A positive separation ratio implies that temperature differences drive the lighter component of the mixture into the direction of higher temperature. That

means that the Soret effect enhances the buoyancy forces that result from the temperature dependence of the density. Convection is therefore established at temperature differences smaller than those needed for pure fluids. The interval of temperature differences that allows convection in a binary mixture but not yet in a pure fluid is called Soret region. Therein convection is driven only because of the presence of the solutal contribution to the buoyancy force. Above this range, i. e. in the Rayleigh region, the thermal part of the buoyancy is most important and the Soret effect is less effective for destabilizing the conductive state.

In the Soret region square-like convection patterns are often found as the primary stable form of convection whereas in pure fluids roll patterns are stable at onset. Such rolls can also be found in binary mixtures, especially at higher heating rates where convection is strong enough to reduce the concentration variations sufficiently by advective mixing. In between there exist two different kinds of crossroll structures: one is stationary and the other one is oscillatory. They are stable where neither rolls nor squares are [4–7]. In this article we summarize our findings about laterally periodic convection structures for positive separation ratios. In Sect. 2 we present the basic equations for binary mixture convection in the Rayleigh–Bénard system and the Galerkin technique we used to investigate the different convection structures numerically. In Sects. 3 – 5 we discuss the properties of rolls, squares, and crossrolls and their range of stability. We conclude in Sect. 6.

2 Numerical Methods

2.1 System and Basic Equations

We consider a horizontal layer of a binary fluid mixture of thickness d in a homogeneous gravitational field, $\boldsymbol{g} = -g\,\boldsymbol{e}_z$. A vertical temperature gradient is imposed by fixing the temperature

$$T = T_0 \pm \frac{\Delta T}{2} \quad \text{at} \quad z = \mp\frac{d}{2}\,, \tag{1}$$

e.g., via highly conducting plates in experiments. Here we consider the plates to be infinitely extended, rigid, and impermeable. T_0 is the mean temperature of the fluid layer.

In the conductive state a linear temperature profile

$$T_{\mathrm{cond}}(z) = T_0 - \frac{\Delta T}{d} z \tag{2}$$

is established. If there is a Soret effect, the temperature gradients generate also a concentration gradient:

$$C_{\mathrm{cond}}(z) = C_0 + S_{\mathrm{T}} C_0 (1 - C_0) \frac{\Delta T}{d} z\,. \tag{3}$$

Here C means the concentration of the lighter component with S_{T} being its Soret coefficient. We will consider the case of negative S_{T}. In this case the lighter

component of the mixture is driven into the direction of higher temperature. Concentration at the bottom is larger in the conductive state for positive ΔT therefore enhancing the density gradient and further destabilizing the fluid layer.

Convection is described in terms of the fields of T, C, velocity $\boldsymbol{u} = (u, v, w)$, total mass density ϱ, and pressure P. In the balance equations connecting these fields we scale lengths and positions by d, time by the vertical thermal diffusion time $d^2/D_{\rm th}$, temperature by $\nu D_{\rm th}/\alpha g d^3$, concentration by $\nu D_{\rm th}/\beta g d^3$, and pressure by $\varrho_0 D_{\rm th}^2/d^2$. Here ϱ_0 is the mean density, $D_{\rm th}$ the thermal diffusivity, ν the kinematic viscosity, and $\alpha = -(1/\rho)\partial\rho/\partial T$ and $\beta = -(1/\rho)\partial\rho/\partial C$ are thermal and solutal expansion coefficients, respectively. Using the Oberbeck–Boussinesq approximation the balance equations read [2,9]

$$\nabla \cdot \boldsymbol{u} = 0 \tag{4a}$$

$$(\partial_t + \boldsymbol{u}\cdot\nabla)\,\boldsymbol{u} = -\nabla p + Pr\,\left[\,(\theta + c)\,\boldsymbol{e}_z + \nabla^2\,\boldsymbol{u}\,\right] \tag{4b}$$

$$(\partial_t + \boldsymbol{u}\cdot\nabla)\,\theta = Ra\,w + \nabla^2\,\theta \tag{4c}$$

$$(\partial_t + \boldsymbol{u}\cdot\nabla)\,c = Ra\,\psi\,w + Le\,\left(\nabla^2\,c - \psi\,\nabla^2\,\theta\right)\ . \tag{4d}$$

Here θ, c, and p are the reduced deviations of temperature, concentration, and pressure, respectively, from the conductive profiles.

The Lewis number Le is the ratio of the concentration diffusivity D to the thermal diffusivity $D_{\rm th}$, therefore measuring the velocity of concentration diffusion. The Prandtl number Pr is the ratio of the momentum diffusivity ν and $D_{\rm th}$:

$$Le = \frac{D}{D_{\rm th}}\ ;\ Pr = \frac{\nu}{D_{\rm th}}\,. \tag{5}$$

The Rayleigh number Ra measures the thermal driving and the separation ratio ψ measures the strength of the Soret coupling between temperature and concentration fields

$$Ra = \frac{\alpha g d^3 \Delta T}{\nu D_{\rm th}}\ ;\ \psi = -\frac{\beta}{\alpha} S_{\rm T} C_0 (1 - C_0)\,. \tag{6}$$

We consider here $S_{\rm T} < 0$, i. e. $\Psi > 0$ for mixtures with $\alpha, \beta > 0$.

The first equation (4a) expresses the fact that the fluid is considered to be incompressible. (4b) – (4d) are the equations of motion for $\boldsymbol{u}$, θ and c. The left hand sides of these equations are the substantial time derivatives of the respective fields. The driving forces entering into the momentum balance equation (4b) are pressure gradients and the buoyancy caused by the temperature and concentration dependence of the density. The remaining term on the right hand side is the momentum diffusion term.

(4c) and (4d) contain also diffusion terms on the right hand side. The off-diagonal term $-Le\,\psi\,\nabla^2\,\theta$ and the term $Ra\,\psi\,w$ in the concentration balance equation (4d) describe the action of the Soret effect, i.e., the generation of concentration currents and concentration gradients by temperature variations.

The Dufour effect, i.e., the driving of temperature currents by concentration variations is of interest only in gas mixtures [9]. But even there it is often small [10].

2.2 Galerkin Method

We are concerned with three-dimensional convection patterns periodic in the x- and y-direction. To describe such patterns with wavenumbers k_x and k_y each field X is expanded as

$$X(x,y,z;t) = \sum_{lmn} X_{lmn}(t) \mathrm{e}^{\mathrm{i}lk_x x} \mathrm{e}^{\mathrm{i}mk_y y} f_n(z) \; . \tag{7}$$

Here l and m are integers and the f_n form a complete system of functions that fits the specific boundary condition for the field X at the plates. To find suitable sets of functions f_n we introduce some new fields. First, two scalar fields Φ and Ψ are defined via

$$\boldsymbol{u} = \nabla \times \nabla \times \Phi \boldsymbol{e}_z + \nabla \times \Psi \boldsymbol{e}_z \; . \tag{8}$$

The structures we want to discuss do not show a horizontal mean flow for mirror symmetry reasons. Then, (8) is the most general expression that fulfills the incompressibility condition (4a) [11].

Second, instead of c we use the field

$$\zeta = c - \psi\theta \tag{9}$$

that allows in a more convenient way to guarantee the impermeability of the horizontal boundaries: The diffusive part of the concentration current, driven by concentration gradients as well as by temperature gradients is given by $-Le\,\nabla(c-\psi\theta)$. At the impermeable plates the vertical component of this current vanishes which requires

$$0 = \partial_z \left(c - \psi\theta\right) = \partial_z \zeta \qquad \text{at } z = \pm 1/2 \; . \tag{10}$$

The advective concentration current vanishes at the plates because there $\mathbf{u} = 0$. The balance equation for ζ is obtained by combining (4c) and (4d).

The boundary conditions for the fields Φ, Ψ, θ, and ζ read

$$\Phi = \partial_z \Phi = \Psi = \theta = \partial_z \zeta = 0 \qquad \text{at } z = \pm 1/2 \; . \tag{11}$$

To expand the fields Ψ, θ, ζ, and Φ vertically we used different orthonormal sets $f_n(z)$ as follows

$$\Psi \text{ and } \theta : f_n(z) = \begin{cases} \sqrt{2}\cos(n\pi z) & n \text{ odd} \\ \sqrt{2}\sin(n\pi z) & n \text{ even} \end{cases} \tag{12a}$$

$$\zeta : f_n(z) = \begin{cases} 1 & n = 0 \\ \sqrt{2}\,\sin(n\pi z) & n \text{ odd} \\ \sqrt{2}\,\cos(n\pi z) & n \neq 0 \text{ even} \end{cases} \tag{12b}$$

$$\Phi : f_n(z) = \begin{cases} C_{\frac{n+1}{2}}(z) & n \text{ odd} \\ S_{\frac{n}{2}}(z) & n \text{ even} \end{cases} \; . \tag{12c}$$

Here C_n and S_n are Chandrasekhar–Reid functions [8].

The balance equations for the new fields are

$$\partial_t \Delta_2 \Psi = Pr \nabla^2 \Delta_2 \Psi + \left\{ \nabla \times \left[(\boldsymbol{u} \cdot \nabla) \boldsymbol{u} \right] \right\}_z \tag{13a}$$

$$\partial_t \nabla^2 \Delta_2 \Phi = Pr \left\{ \nabla^4 \Delta_2 \Phi - \Delta_2 \left[(1+\psi)\,\theta + \zeta \right] \right\} - \left\{ \nabla \times \nabla \times \left[(\boldsymbol{u} \cdot \nabla) \boldsymbol{u} \right] \right\}_z \tag{13b}$$

$$(\partial_t + \boldsymbol{u} \cdot \nabla)\,\theta = -Ra\, \Delta_2 \Phi + \nabla^2 \theta \tag{13c}$$

$$(\partial_t + \boldsymbol{u} \cdot \nabla)\,\zeta = Le \nabla^2 \zeta - \psi \nabla^2 \theta \; . \tag{13d}$$

Here $\Delta_2 = \partial_x^2 + \partial_y^2$.

By inserting the ansatz (7) for each field into the balance equations and projecting them onto the basic functions one gets a nonlinear algebraic system of equations of the form

$$A_{\kappa\mu} \partial_t X_\mu = B_{\kappa\mu} X_\mu + C_{\kappa\mu\nu} X_\mu X_\nu \; . \tag{14}$$

For simplicity amplitudes are labelled here by a single Greek index and the summation convention is implied in (14) with $A_{\kappa\mu}$, $B_{\kappa\mu}$, and $C_{\kappa\mu\nu}$ being constant coefficients.

The number of modes has to be truncated to get a finite number of equations as discussed later on. For stationary convection structures the left hand side of (14) vanishes and the solution can be found using a multidimensional Newton method.

2.3 Stability Analysis

To make a full stability analysis one has to check the stability of the patterns against perturbations with arbitrary wavevector $d\boldsymbol{e}_x + b\boldsymbol{e}_y$. To do so one has to introduce a Floquet term writing out the perturbation as

$$\delta X(x,y,z;t) = \mathrm{e}^{\mathrm{i}dx + \mathrm{i}by} \mathrm{e}^{st} \sum_{lmn} \delta X_{lmn} \mathrm{e}^{\mathrm{i}lk_x x + \mathrm{i}mk_y y} f_n(z) \; . \tag{15}$$

Such a perturbation is added to the known solution the stability of which is to be tested and inserted into the balance equations. After linearizing and projecting one gets a linear eigenvalue problem of the form

$$s A_{\kappa\mu} \delta X_\mu = B_{\kappa\mu} \delta X_\mu \; . \tag{16}$$

with constant coefficients $A_{\kappa\mu}$ and $B_{\kappa\mu}$. The aforementioned solution, i.e., the convective structure described by it is stable if every eigenvalue s has a negative real part for every d and b.

The symmetry of the convective pattern discussed above can under some circumstances be used to get separated classes of possible eigenvectors representing the perturbations. That means the eigenvalue problem can be reduced to finding the eigenvalues of two matrices of about half of the size. Because evaluating the eigenvalues of a matrix is a $O(N^3)$-process this always implies a reduction of the computation time.

2.4 Parameter Space

In pure fluids convection in the Rayleigh–Bénard system starts at a critical Rayleigh number $Ra_c^0 = Ra_c(\psi = 0) = 1707.762$ and a wavenumber $k_c^0 = k_c(\psi = 0) = 3.117$ [8]. In binary mixtures with positive separation ratios that we are dealing with, the critical Rayleigh number is smaller, $Ra_c(\psi > 0) < Ra_c^0$, since the solutal contribution to the quiescent state's buoyancy force enhances the latter. Thus a smaller thermal driving, i.e., a smaller Rayleigh number suffices to reach the critical buoyancy force size for onset of convection. The critical wavenumber is also somewhat lower: $k_c(\psi > 0) < k_c^0$ [12]. When presenting our results we shall use the reduced Rayleigh number

$$r = \frac{Ra}{Ra_c^0} \,. \tag{17}$$

The convection above onset depends on the three parameters ψ, Le, and Pr. These parameters depend on the components of the mixture and the mean values of temperature and concentration. For alcohol-water for example, ψ may assume values between -0.6 and 0.3. Here the Lewis number $Le = 0.01$ or smaller whereas $Le \approx 1$ is typical for gas mixtures. A typical Prandtl number for liquid mixtures is $Pr = 10$, in gas mixtures $Pr = 0.1...1$.

3 Rolls

In pure fluids, convection in the form of parallel rolls is a stable form of convection directly above onset for all values of Pr [13], although they compete with spiral defect chaos at low Prandtl numbers where the latter structure has a larger basin of attraction [14]. In binary mixtures, they exist also as stable patterns above Ra_c for all positive ψ if Le is large enough to equilibrate the concentration sufficiently. The required value of Le depends mainly on the strength of the Soret effect but also on the Prandtl number. The rolls lose stability against squares at onset if Le is too small, especially for strong Soret coupling [15].

3.1 Technical Remarks

Calculating the fixed point solutions and analyzing their stability requires less numerical effort than for 3D structures. Only X_{l0n}-modes have to be taken into account and $\Psi \equiv 0$. Mirror symmetry in the lateral direction allows to set $X_{l0n} = X_{-l0n}$ so that the lateral functions $\mathrm{e}^{\pm \mathrm{i}klx}$ can be replaced by $\cos(klx)$. In addition the roll pattern is antisymmetric under reflection at the plane $z = 0$ combined with a translation by half a wavelength in x-direction. This mirror glide symmetry enforces half of the amplitudes to be zero, e. g. all amplitudes Φ_{l0n} where $l + n$ is an odd number.

To perform the stability analysis of rolls one determines the growth behavior of perturbations of the form

$$\delta X(x, y, z; t) = \mathrm{e}^{\mathrm{i}dx + \mathrm{i}by} \mathrm{e}^{st} \sum_{ln} \delta X_{l0n} \mathrm{e}^{\mathrm{i}lkx} f_n(z) \,. \tag{18}$$

Because of the periodicity of the patterns in x and its mirror symmetry it suffices to consider $d \in [0, k/2]$. In y-direction, however, all perturbation wavenumbers, say, $b \geq 0$ have to be investigated. For a discussion of the effect of mean flow perturbations, e. g., $\delta\Phi_{00n}$ we refer to [16].

The linear system of equations (18) always separates into two subsystems of perturbations δX_{l0n} that belong to modes with amplitudes X_{l0n} that are antisymmetric or symmetric under the mirror glide operation $(x, z) \rightarrow (x + \lambda/2, -z)$. E. g. all perturbations with amplitudes $\delta\Phi_{l0n}$ with even $l + n$ belong to one set, while the perturbations with odd $l + n$ belong to the other.

In special cases the system of equations can be separated even further. For $d = 0$ the perturbations can be divided into those that are symmetric and those that are antisymmetric under the operation $x \rightarrow -x$. Furthermore, if $b = 0$ then the perturbations contain either no or only $\delta\Psi$-amplitudes. This is also of practical interest, since some instabilities are most critical in these special cases.

The sets of modes taken into account in the Galerkin procedure were chosen as follows: We defined a maximal mode index N and neglected all modes X_{l0n} or δX_{l0n} with $|l|+n > N_1$ for Φ- and Ψ-fields and $|l|+n > N_2$ for θ- and ζ-fields. Here $N_2 = 2N_1$.

3.2 Numerical Results

A quantitative description of the fixed point solutions and the stability behavior in binary mixtures requires in some cases sets of modes that are much larger than those needed for pure fluids. This is because the strong anharmonic narrow boundary layer behavior of the ζ-field for small Le and large r. For the most anharmonic roll structures at $r \approx 1.5$, $Le < 0.01$, and $\psi = 0.15$ that we have investigated expansions up to $N_2 = 40$ were needed. Although the velocity and temperature field are much smoother, a consistent description of the latter requires then also high θ-modes as discussed in [17,18]. This is much more than for pure fluids, where truncations with $N \leq 8$ are sufficient to describe the stability behavior quantitatively even at large r.

Roll Solutions

We will discuss the fixed point solutions by focusing on the mode intensity $|\Phi_{101}|^2$ at $k = k_c^0$ as order parameter (see Fig. 1). The relation to the vertical velocity w is $k^2\Phi_{101} = w_{101}$. It is useful to start with considering solutions for small Le. In this case, two different convection regimes can be distinguished. For $r < 1$, in the Soret regime, the applied temperature gradients cause convection only indirectly, by generating concentration and therefore density gradients via the Soret effect. The convection amplitudes are very small here. This changes in the Rayleigh regime, where the temperature gradients cause the necessary density gradients to develop convection also directly. $|\Phi_{101}|^2(r)$ strongly curves upward and $|\Phi_{101}|^2$ assumes values comparable to those of pure fluid convection, since concentration is more and more equilibrated.

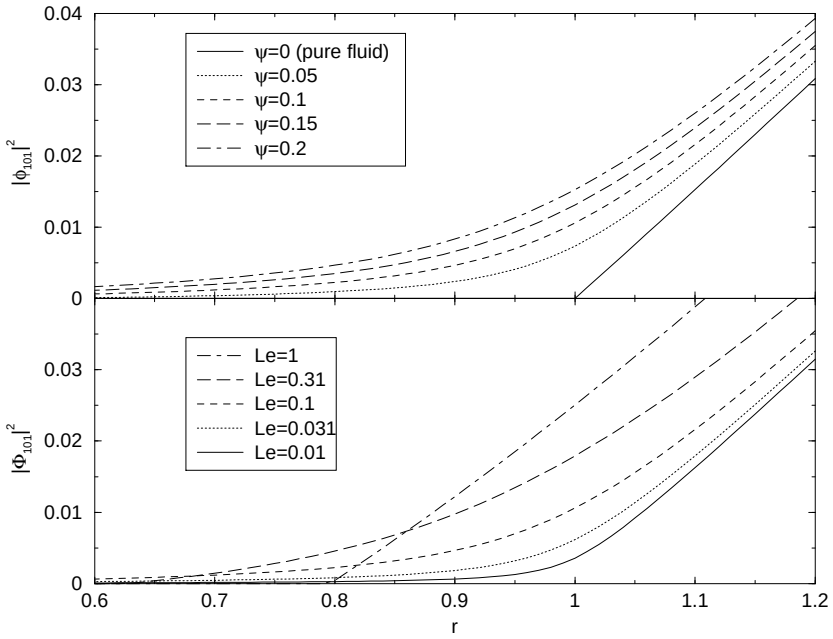

Fig. 1. Mode intensity $|\Phi_{101}|^2$ of roll solutions as a function of r for $k = k_c^0$ and $Pr = 10$. Above: for $Le = 0.1$ and different ψ. Below: for $\psi = 0.1$ and different Le

The transition between Soret and Rayleigh region is especially sharp if ψ is also small. It is also present for larger Le, but more smooth. It vanishes for $Le \approx 1$. The knowledge of these features will be helpful for a qualitative understanding of the stability behavior.

Stability Properties of Rolls

The stability boundaries of roll patterns in pure fluids are known since the pioneering work of Busse and his coworkers [13]. At small Rayleigh numbers there exist five different instability mechanisms giving rise to five different stability boundaries that limit the region of stable rolls in the (Ra, k, Pr)-parameter space. At small Prandtl numbers the Eckhaus (EC), the skewed varicose (SV), and the oscillatory mechanism (OS) are the important instabilities [19]. At higher Prandtl numbers the zigzag (ZZ) and the crossroll (CR) mechanisms dominate [20]. Properties and symmetries of these perturbations are discussed in [21]. These five instabilities of roll patterns are the same as those that can be found in binary mixtures. A more detailed discussion of the symmetries and other features of these mechanisms can be found in [16].

The central qualitative difference between roll structures in pure fluids and binary mixtures concerning their stability is certainly their loss of stability in mixtures at onset in a wide range of parameter space. However, roll structures

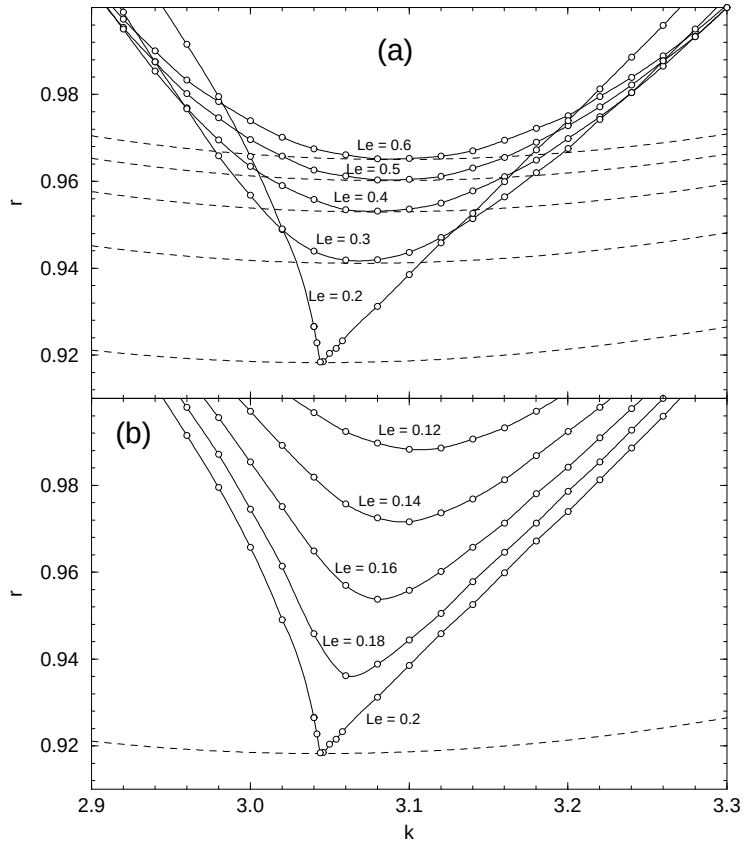

Fig. 2. CR instability boundaries (solid lines) of rolls in the Soret region for $Pr = 10$, $\psi = 0.01$ and several values of Le. Rolls are stable against CR-perturbations above the solid lines. (a): For $Le \geq 0.2$ the CR boundaries touch the neutral curve (dashed lines) in the critical point. (b): For $Le < 0.2$ the neutral curve goes further down (not shown) and is disconnected from the CR boundaries. Then rolls are not stable at the critical point anymore

do in general still exist in mixtures as stable structures for these parameters, not at onset, but at larger r. Figure 2 shows the CR instability boundaries of rolls in a parameter interval where an exchange of stability between rolls and squares at onset is predicted in [15]. One sees that the curvature of the CR boundary at the critical point diverges – a feature that follows also from cubic amplitude equations, see [16] – when this exchange occurs. For the parameters $Pr = 10, \psi = 0.01$ of Fig. 2 the exchange occurs at $Le = 0.2$. Decreasing Le below this value the neutral stability curve (dashed line in Fig. 2) drops further down in r (not shown in Fig. 2b) while the CR instability boundary disconnects

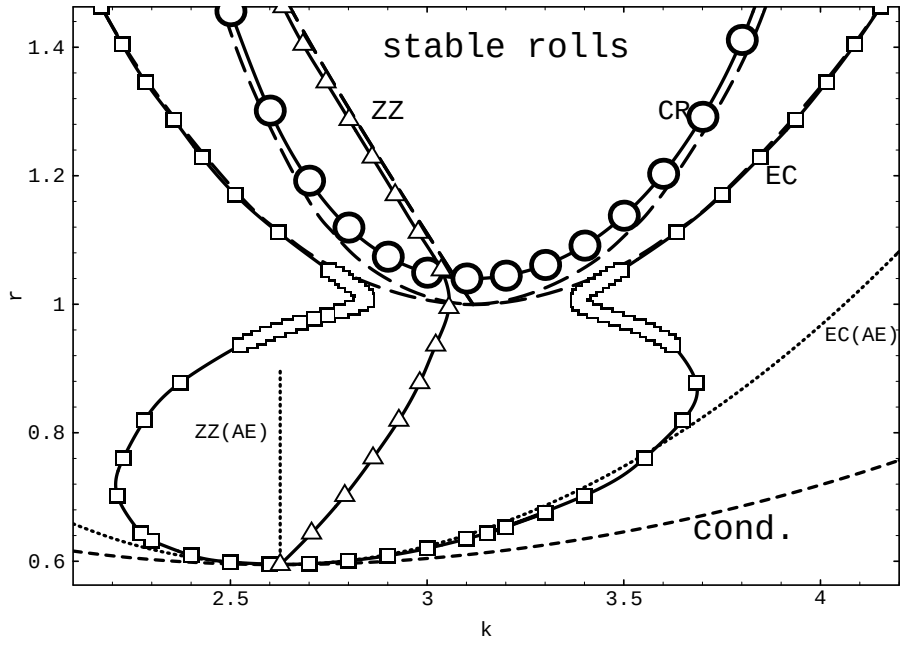

Fig. 3. Stability boundaries of rolls. Solid lines with open symbols refer to a mixture with $Pr = 7$, $\psi = 0.01$, and $Le = 0.025$. The corresponding boundaries in a pure fluid with $Pr = 7$ are the long dashed curves. Dotted curves labelled EC(AE) and ZZ(AE) are predictions of cubic amplitude equations for the EC and ZZ boundaries of the mixture, respectively. The conductive state is stable below the short–dashed curve labelled cond.

from the neutral stability curve and moves up in r. Above the CR boundary rolls are still stable against CR perturbations.

The rolls could still be unstable there against other perturbations but we found the minimum of the CR boundary always to be the minimal Rayleigh number above which stable rolls exist. Only at $\psi = 0.15$, $Pr < 0.2$ and $Le < 0.015$ we found regions where rolls seem to be unstable everywhere in the (k, r)-plane. The two branches of the CR boundary meet again at higher r near this region and limit an oval region of CR-stable rolls from below and also *above*. The oval region gets smaller by reducing Le or Pr until the region of stable rolls vanishes. The experimental observation of this behavior might be difficult because it occurs in a region of the parameter space that is not accessible by ordinary fluid mixtures.

We have calculated all stability boundaries at small r for different values of Le, ψ, and Pr. Concerning the stability behavior of the roll structures one sees that in the Rayleigh region, $r > 1$, where the concentration field is nearly uniform the binary mixture behaves like a pure fluid. As for the fixed points, the transition between Soret and Rayleigh region is very sharp at small Le and

ψ. An example for such a behavior is given in Fig. 3. Here only the EC, CR, and ZZ boundaries are of importance. In the Rayleigh region of Fig. 3 the CR, ZZ, and EC boundaries of the mixture (full lines with circles, triangles, and squares, respectively) are lying close to the corresponding boundaries of the pure fluid (long-dashed lines). Note in particular the vase-like form of the EC boundary $r_{\mathrm{EC}}(k)$ and the dent in the ZZ boundary $r_{\mathrm{ZZ}}(k)$: Closer to onset ($r_{\mathrm{c}} \simeq 0.6, k_{\mathrm{c}} \simeq 2.6$ in Fig. 3), i.e., in the Soret regime $r_{\mathrm{EC}}(k)$ opens up parabolically and $r_{\mathrm{ZZ}}(k)$ comes out of the critical point linearly with *positive* slope. However, in the crossover range $r \sim 1$ between Soret and Rayleigh regime the curve $r_{\mathrm{EC}}(k)$ pinches inwards and develops a waist such as to follow in the Rayleigh regime the parabolic shape of the EC curve of the pure fluid that starts out at $k_{\mathrm{c}}^0 \simeq 3.1, r_{\mathrm{c}}^0 = 1$. Similarly $r_{\mathrm{ZZ}}(k)$ bends in the crossover range towards small k to follow then the ZZ boundary of the pure fluid that shows *negative* slope.

Figure 4 show that this transition between Soret and Rayleigh region that causes the vase-like structure of the EC boundary and the sharp bend of the ZZ boundary is smoother for larger Le or ψ. For $Le = 1$, the stability balloon does not qualitatively differ from its pure fluid counterpart.

4 Squares

Convection in square patterns is a fixed point solution that bifurcates out of the conductive state and that coexists with the roll solution. For parameter combinations where rolls are not stable at onset, square structures gain stability. They lose stability at higher r, roughly at the boundary between Soret and Rayleigh region.

4.1 Technical Remarks

Squares have the same symmetry plane at $x = 0$ as rolls and an additional mirror plane at $y = 0$. Furthermore, squares show also a mirror glide symmetry. Here, however, the symmetry transformation consists of a reflection at the plane $z = 0$ combined with a translation by half a wavelength in x- *and* y-direction. To describe these three-dimensional patterns the Ψ-field cannot be neglected. We also mention that in contrast to the other fields Ψ is odd in x and y and has positive parity under the mirror glide operation thereby reflecting the symmetries of the velocity field. A further reduction of the number of mode occurs since square patterns are invariant under rotation by 90° mapping the x- onto the y-directions and vice versa. Amplitudes like Φ_{lmn} and Φ_{mln} are the same. This is also true for θ and ζ. Again Ψ is different. Here $\Psi_{lmn} = -\Psi_{mln}$.

Because the amount of computational power needed to make a full stability analysis of these three-dimensional structures is too large, we will discuss perturbations only for periodic boundary conditions, i. e., $d = b = 0$. Here again a separation of perturbations is possible into those that change sign or not under the mirror glide operation. Furthermore, the stability problem is invariant under $x \to -x$ and $y \to -y$. Thus one can distinguish between perturbations that are

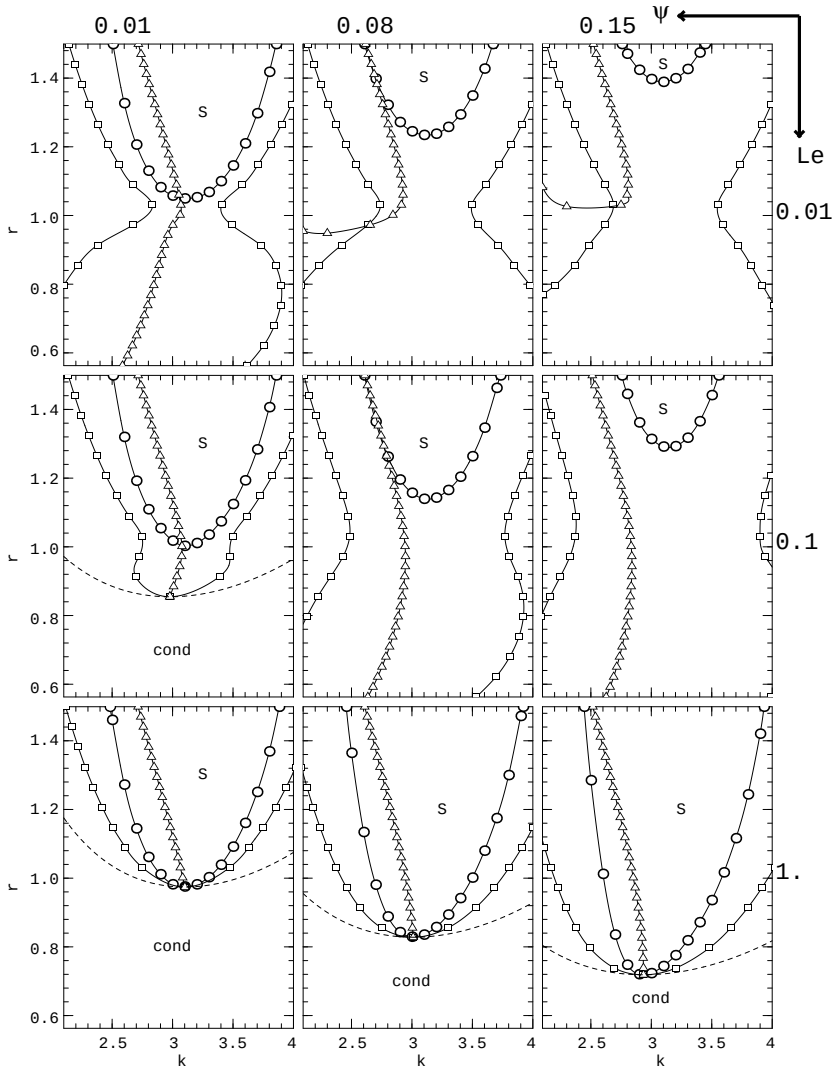

Fig. 4. Crossections of the stability balloon of rolls in the $k - r$ plane at $Pr = 10$. Open circles: CR, open squares: EC, open triangles: ZZ. S denotes the region of stable rolls

even in x and y, odd in x and y, or even in x and odd in y (or equivalently odd in x and even in y). If the perturbations have the same symmetry in both directions one can in the case of squares finally make use of a last symmetry property and

separate between perturbations that are symmetric or antisymmetric under the exchange of the x- and y-direction.

The modes taken into account for the Galerkin procedure were chosen in a way analogous to the roll case: X_{lmn} and δX_{lmn} were neglected, if $|l| + |m| + n$ was larger than N_1 or N_2 respectively. Since square structures are stable mainly below $r = 1$ and the boundary layers are less narrow compared to the coexisting roll solutions (see below), values of $N_2 \leq 20$ were sufficient.

4.2 Numerical Results

Square Solutions

The convection patterns of squares resemble linear superposition of two perpendicular sets of rolls. The intensities of the leading modes $\Phi^{\mathrm{S}}_{101} = \Phi^{\mathrm{S}}_{011}$ of the square solutions show qualitatively the same r-dependence as Φ^{R}_{101} for roll solutions but are always smaller. Arguments based on amplitude equations show however, that $|\Phi^{\mathrm{S}}_{101}|^2 + |\Phi^{\mathrm{S}}_{011}|^2 > |\Phi^{\mathrm{R}}_{101}|^2$ near onset if and only if squares are stable there. But this is no longer true at higher r where the solutions are such that $|\Phi^{\mathrm{S}}_{101}|^2 + |\Phi^{\mathrm{S}}_{011}|^2 < |\Phi^{\mathrm{R}}_{101}|^2$. This change takes place before squares lose stability.

In Fig. 5 we show the concentration distribution of square convection for two parameter combinations that are representative for liquid and gas mixtures. This plot and the concentration field structure of rolls and squares in a vertical cross section shows a characteristic boundary layer and plume behavior at small Le. Such structures occur when advective mixing is large compared to diffusion in the bulk of the fluid. Consequently the boundary layers and plumes are more pronounced in rolls than in squares since the leading velocity amplitudes are greater for the former. Thus squares with their broader boundary layers are much smoother structures than rolls at the same parameters. The practically harmonic velocity and temperature fields are not shown.

Stability Properties of Squares

Performing the stability analysis of squares we had to restrict ourselves to the case $d = b = 0$ where the perturbations separate into different symmetry classes. Because both squares and rolls can be described as even in x and y and as mirror glide antisymmetric, one expects a perturbation that destabilizes the squares and favors the rolls to fulfill these symmetries, too. However such a perturbation should break the symmetry $x \leftrightarrow y$. We actually always found the most critical perturbation to fall into this symmetry class. Other perturbations that break the mirror symmetry in x- or y-direction are less critical.

Figure 6 shows typical examples for the stability region of squares. The left and right side of the stability boundaries should not be taken too serious – presumably square structures are destabilized earlier by instabilities with finite b or d that tune the wavenumber and that are not considered here.

Even if squares are stable at onset they always lose their stability against a roll pattern at higher r. Furthermore, for certain parameters there does also exist

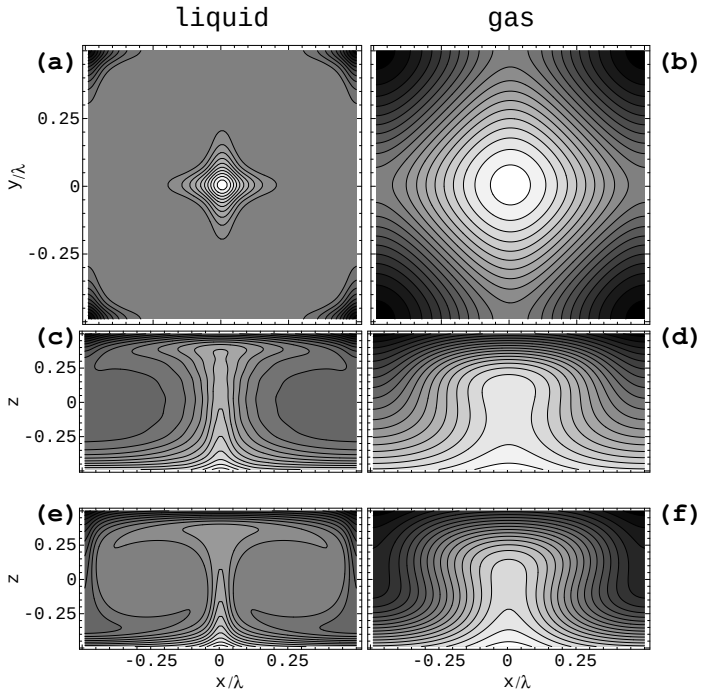

Fig. 5. Structural properties of square (a-d) and roll (e,f) convection for representative liquid parameters ($Le = 0.01$, $Pr = 10$, left column) and gas parameters ($Le = Pr = 1$, right column) at $r = 1, \psi = 0.15$. In (a,b) the concentration distribution of squares at mid height, $z = 0$, is shown. In (c-f) we show the concentration distribution in a vertical cross section at $y = 0$. The largest vertical upflow is at $x = y = 0$

a band of r-values where neither squares nor rolls are stable. Therein crossrolls or oscillations appear as stable patterns.

5 Crossrolls

Crossrolls are 3D convection patterns that show the same symmetries as squares except the $x \leftrightarrow y$ symmetry. As squares, they can be qualitatively described as superpositions of perpendicular roll patterns. But in the case of crossrolls the amplitudes Φ_{101} and Φ_{011} of the x- and y-rolls are not the same.

Crossroll structures appear in two modifications: as stationary and as oscillatory crossrolls. For the latter, the amplitudes of x- and y-rolls are time dependent.

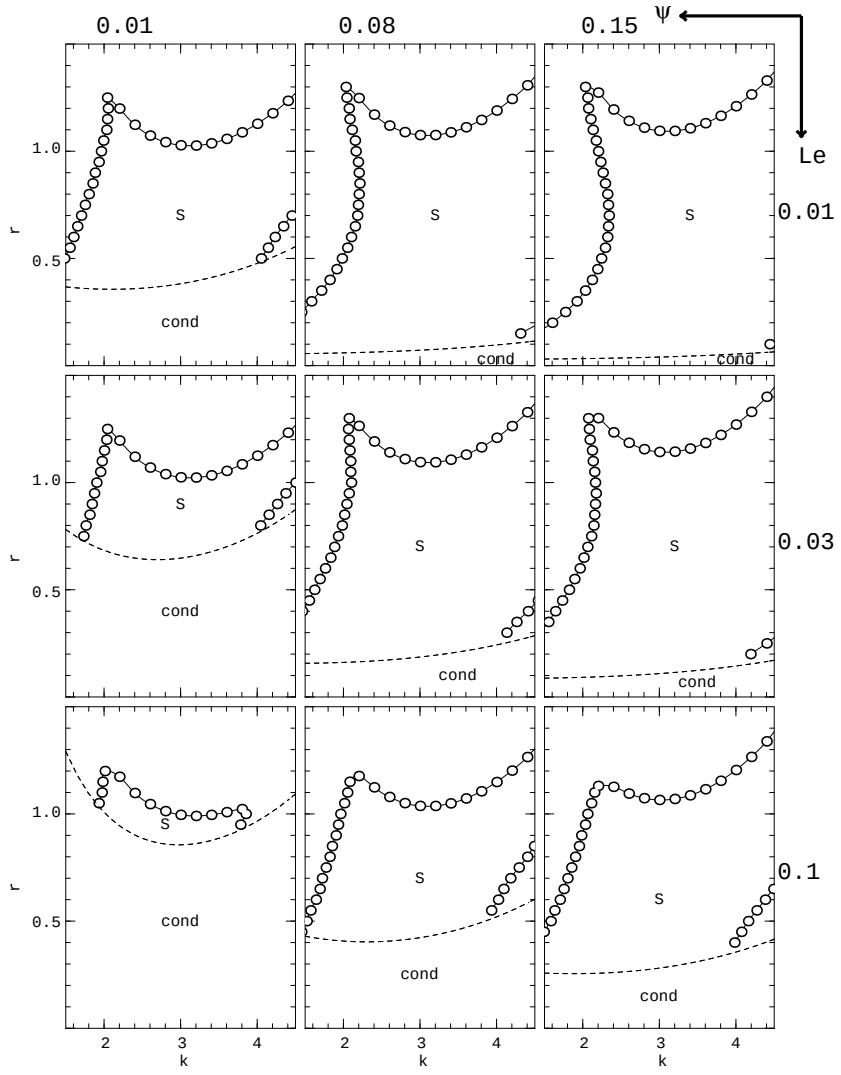

Fig. 6. Crossections of the stability balloon of squares in the $k - r$ plane for $Pr = 10$ obtained from a restricted stability analysis as explained in the text. S denotes the region of stable squares

5.1 Technical Remarks

The numerical investigations of the crossroll structures were performed as in the case of squares except that modes like X_{lmn} and X_{mln} could not be identified

anymore due to the lack of the $x \leftrightarrow y$ symmetry. For $b = d = 0$ instabilities are either mirror glide symmetric or antisymmetric. They are either even or odd in the x- and the y-direction. We used expansions up to $N_2 = 20$ to investigate these structures. The time-dependent structures were investigated via direct numerical integration of the equations of motion for the modes.

5.2 Numerical Results

Stationary crossrolls exist at parameters Pr, L, ψ if squares are stable at onset. Then, they appear in the r-range were squares are already and rolls are still unstable. Oscillatory crossrolls exist only at small Le. The connection between the different structures can be extracted from the bifurcation diagram in Fig. 7. For the parameters $Pr = 27$, $Le = 0.0047$, and $\psi = 0.23$ taken from [5], all four kinds of patterns exist. For the calculation of the fixed points a model with $N_2 = 10$ was used, the bifurcation diagram is therefore only qualitatively correct at higher r.

Stationary Crossrolls

We will first ignore the crossroll solutions of the oscillatory type and concentrate on the stationary patterns. At onset squares with $|\Phi_{101}|^2 = |\Phi_{011}|^2$ are the stable structure. The coexisting roll branch is unstable. At about $r = 1.11$ a new type of solutions bifurcates out of the square branch, the stationary crossrolls. In this r-range neither squares nor rolls are stable. For the crossroll structures the two important mode intensities are different, say $|\Phi_{101}|^2 > |\Phi_{011}|^2$. The difference between these intensities grows until $|\Phi_{011}|^2 = 0$ and $|\Phi_{101}|^2$ touches the roll branch at another bifurcation point at $r \approx 1.24$. The crossrolls transfers their stability to the rolls here.

The stationary crossrolls exist always inside an intermediate r-range if squares are stable at onset. The oscillatory type appears only at very small Le as in Fig. 7. If these solutions are absent, the squares transfer their stability directly to the stationary crossroll branch, leading to a sequence squares – stationary crossrolls – rolls of stable structures for increasing r. In particular, the stability boundaries that limit the region of stable squares in Fig. 6 are all of the type leading to stationary rolls: oscillatory crossrolls do not exist for these parameters.

Oscillatory Crossrolls

But for the parameters in Fig. 7 the bifurcation behavior is more complicated. The squares lose their stability already at $r \approx 1.08$ before the stationary crossrolls emerge. At this point oscillatory crossrolls grow out of the square state in a supercritical Hopf bifurcation. The stationary crossrolls that appear at $r = 1.11$ remain unstable until $r \approx 1.14$.

Fig. 8 shows for several Rayleigh numbers that $|\Phi_{101}|^2(t)$ and $|\Phi_{011}|^2(t)$ oscillate in opposite phase around a common mean value given by the unstable

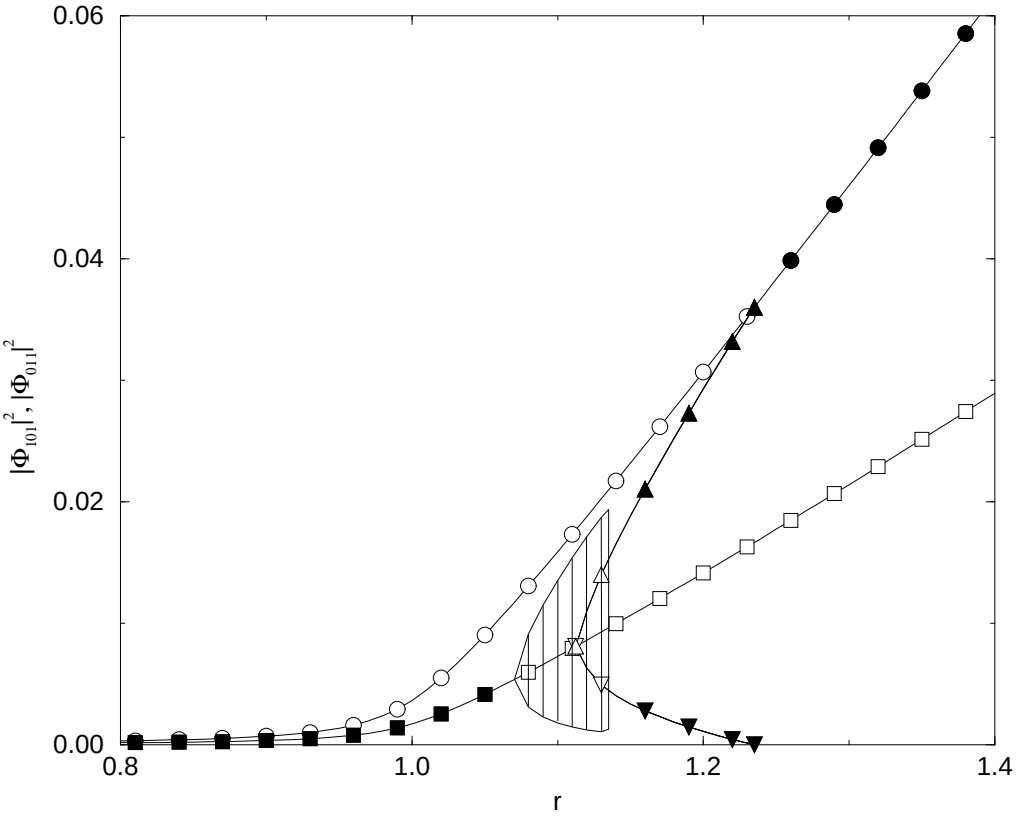

Fig. 7. Bifurcation diagram of x-roll intensity and y-roll intensity versus r for squares (squares), rolls (circles), stationary (triangles), and oscillatory crossrolls. Filled (open) symbols denote stable (unstable) states. Full lines delimiting the hatched area mark maxima and minima of oscillations of $|\Phi_{101}|^2$ and $|\Phi_{011}|^2$. The parameters are [5] $\psi = 0.23$, $L = 0.0045$, $Pr = 27$, and $k = \pi$

square state. The x-roll intensity of the pulsating pattern grows or decreases on cost of the y-roll intensity, however, without ever going to zero. Thus the two roll sets never die out completely or reverse their turning direction during the oscillations. Close to the Hopf bifurcation the oscillations are harmonic and of small amplitude (Fig. 8a). With increasing r the frequency decreases roughly linearly [5]. Furthermore, and more importantly, with increasing amplitude the oscillation becomes more anharmonic and relaxational in Fig. 8b, c; see also Ref. [4,5]: While the system rapidly sweeps through the square state it spends more and more time in the vicinity of the roll state. The change from harmonic in Fig. 8a to strongly relaxational oscillations in Fig. 8c is also documented in

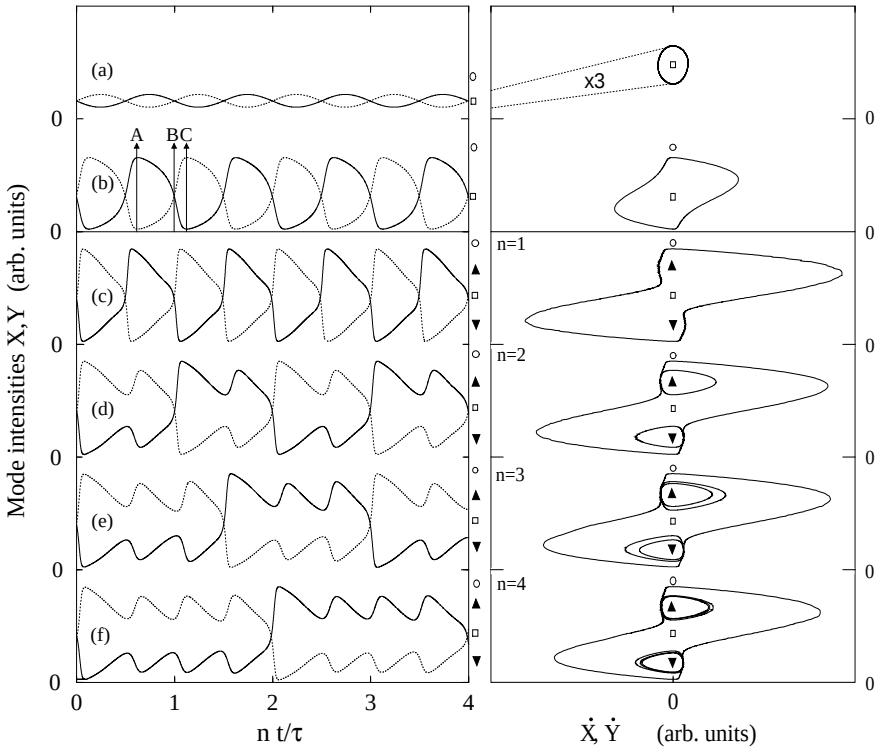

Fig. 8. Evolution of the oscillatory dynamics with increasing r from top to bottom. Parameters as in Fig. 7. (a) and (b) are states located shortly above the Hopf threshold and right below the crossroll bifurcation, respectively. (c) – (f) are SC states. The right column contains phase space plots of $X \sim |\Phi_{101}|^2$ and $Y \sim |\Phi_{011}|^2$ versus their time derivatives for the intensities X, Y shown in the left column with arbitrary common units versus reduced time nt/τ. In the SC states n is the number of windings around each of the stable crossroll fixed points (triangles). Squares and circles indicate unstable square and roll states, respectively

the right column of Fig. 8. There we show phase space plots associated with the time histories of $|\Phi_{101}|^2$, $|\Phi_{011}|^2$ in the left column.

At larger r the system gets attracted into one of the crossroll fixed points that have become stable shortly before oscillatory crossrolls cease to exist in Fig. 7. In this interval we have observed a novel subharmonic bifurcation cascade (SC) in which the crossroll attractors entrain the oscillations: First the crossroll attractors deform the phase trajectory (Fig. 8c). Then with increasing r the oscillations execute an increasing number of windings around the crossroll states. In Figs. 8c – f the winding number around a crossroll fixed point increases from $n = 1$ to $n = 4$ and the period τ of the oscillations increases from $2\pi/\omega$ to $2\pi n/\omega$ in integer steps. This increase of the winding number in the SC continues beyond

$n = 4$; we have found also $n = 5$. However, the control parameter interval δr_n for an n-cycle becomes so narrow – $\delta r_n \cong (1.6, 0.6, 0.2)10^{-4}$ for $n = (2, 3, 4)$ – that our numerical resources were not sufficient to resolve the SC further. But we think that the SC is a robust, experimentally accessible phenomenon; Ref. [4] contains a hint for a 2-cycle. Beyond the SC interval in the system gets attracted into one of the crossroll fixed points. The transition between the oscillations and the crossroll state is slightly hysteretic. Upon reducing r the system remains in the crossroll state until below the SC interval and then a transition to an $n = 1$ oscillation occurs. So in a small r-interval there is bistable coexistence of oscillations and stationary crossrolls.

6 Conclusion

We reviewed our findings of Rayleigh–Bénard convection in binary mixtures with positive Soret effect. In this case the lighter component of the mixture is driven into the direction of higher temperature. The enhanced density gradient leads to a convective instability at smaller temperature differences than in the pure fluid case. Convection at positive ψ shows a rich variety of stable structures at moderate $r \leq 1.5$.

Using the Galerkin technique, we investigated two- and three-dimensional laterally periodic patterns as rolls, squares, and stationary and oscillatory crossrolls and determined their stability behavior. All these patterns are realized as stable convection structures somewhere in parameter space. The numerical examination of convection in liquid binary mixtures is in general much more difficult compared to pure fluids since small values of the Lewis number $Le \leq 0.01$ lead to a pronounced narrow boundary layer behavior of the concentration field. This is especially the case for rolls whereas squares are somewhat smoother. Nevertheless we had to restrict the stability analysis of the three-dimensional structures to perturbations with the same wave number.

Squares and rolls coexist as convective solutions above onset. The square symmetry requires that the main velocity modes are equal: $|\Phi_{101}| = |\Phi_{011}|$. For the two-dimensional rolls on the other hand one of these amplitudes, say $|\Phi_{011}|$ is zero. Squares are stable in the Soret region if Le is sufficiently small. They transfer their stability to crossrolls at higher r. If Le is not too small, only stationary crossrolls exist. As squares, they can be described as linear superpositions of roll structures. For them however, $|\Phi_{101}| > |\Phi_{011}|$ or vice versa. With increasing r the smaller amplitude tends to zero until the crossroll branch ends on the now stable roll branch in the bifurcation diagram.

At very small Le there exists also a branch of oscillatory crossrolls that emerges out of the square branch in a supercritical Hopf bifurcation at smaller r than the branch of the stationary type. In the oscillatory crossrolls $|\Phi_{101}|^2(t)$ and $|\Phi_{011}|^2(t)$ oscillate in opposite phase around a common mean value given by the unstable square state. At higher r the oscillatory crossrolls disappear in a subharmonic bifurcation cascade and the stationary ones gain stability.

At higher Le roll structures are stable directly above onset and crossrolls structures do not appear. The analysis of the rolls shows that in the explored parameter range only the basic mechanisms of instability occur that are already known from the pure fluid, namely the Eckhaus, zigzag, crossroll, oscillatory, and skewed varicose mechanism. When the Soret region is small, the stability balloon of the mixtures resembles the Busse balloon for the pure fluid. However, at small Le when the Soret region is large the situation is different. The fixed point solutions show a sharp transition between the two regimes. The convection amplitudes are very small in the Soret regime. But near $r = 1$ they increase strongly and become comparable to those of the pure fluid convection. The stability boundaries of roll convection show a similar transition here. In the Rayleigh region the boundaries are close to the boundaries of the pure fluid. But upon reducing the Rayleigh number the boundaries begin to deviate from their pure fluid counterparts. Near onset they finally agree with the predictions of the amplitude equations for the mixtures.

References

1. M. C. Cross, P. C. Hohenberg: Rev. Mod. Phys. **49**, 581 (1993)
2. J. K. Platten, J. C. Legros: *Convection in Liquids.* (Springer, New York 1984)
3. M. Lücke, W. Barten, P. Büchel, C. Fütterer, St. Hollinger, Ch. Jung: 'Pattern formation in binary fluid convection and in systems with throughflow'. In: *Evolution of spontaneous structures in continuous systems* ed. by F. H. Busse, S. C. Müller. Lecture Notes in Physics **55**, 127. (Springer, Berlin, Heidelberg 1998)
4. P. Le Gal, A. Pocheau, V. Croquette: Phys. Rev. Lett. **54**, 2501 (1985)
5. E. Moses, V. Steinberg: Phys. Rev. Lett. **57**, 2018 (1986); Phys. Rev. A **43**, 707 (1991)
6. M. A. Dominguez-Lerma, G. Ahlers, D. S. Cannell: Phys. Rev. A **52**, 6159 (1995)
7. Ch. Jung, B. Huke, M. Lücke: Phys. Rev. Lett. **81**, 3651 (1998)
8. S. Chandrasekhar: *Hydrodynamic and hydromagnetic stability*, Appendix V (Dover, 1981)
9. W. Hort, S. Linz, M. Lücke: Phys. Rev. A **45**, 3737 (1992)
10. J. L. Liu, G. Ahlers: Phys. Rev. E **55**, 6950 (1997)
11. R. M. Clever, F. H. Busse: J. Fluid Mech. **198**, 345 (1989)
12. E. Knobloch, D. R. Moore: Phys. Rev. A **37**, 860 (1988)
13. F. H. Busse: Rep. Prog. Phys. **41**, 1929 (1978)
14. J. L. Liu, G. Ahlers: Phys. Rev. Lett. **77**, 3126 (1996)
15. T. Clune, E. Knobloch: Phys. Rev. A **44**, 8084 (1991)
16. B. Huke, M. Lücke, P. Büchel, Ch. Jung: J. Fluid Mech. **408**, 121 (2000)
17. St. Hollinger, M. Lücke: Phys. Rev. E **57**, 4238 (1998)
18. St. Hollinger: Theorie der ausgedehnten stationären und wandernden Konvektion in binären Fluidmischungen. PhD thesis, Universität des Saarlandes, Saarbrücken (1996)
19. R. M. Clever, F. H. Busse: Phys. Fluids A **2**, 334 (1990)
20. F. H. Busse: Journal of Mathematics and Physics **46**, 140 (1967)
21. E. W. Bolton, F. H. Busse, R. M. Clever: J. Fluid Mech. **164**, 469 (1985)

Glossary

b	wave vector deviation in y
c	concentration deviation
C	concentration
C_0	mean concentration
C_{cond}	concentration in conductive state
CR	crossroll instability
d	wave vector deviation in x, also plate distance
$\mathbf{e}_x, \mathbf{e}_y, \mathbf{e}_z$	unit vectors
EC	Eckhaus instability
$\boldsymbol{g}$	gravitational field
k	wave number
k_x	wave number in x
k_y	wave number in y
k_{c}	critical wave number
k_{c}^0	critical wave number for pure fluid
OS	oscillatory instability
p	pressure deviation
P	pressure
r	reduced Rayleigh number
Ra_{c}	critical Rayleigh number
Ra_{c}^0	critical Rayleigh number for pure fluid
s	growth rate
SV	skeved varicose instability
T_0	mean temperature
T_{cond}	temperature in conductive state
ΔT	temperature difference
u	velocity, x component
v	velocity, y component
w	velocity, z component
X	arbitrary field
X_{lmn}	field mode
δX	perturbation in field X
δX_{lmn}	perturbation mode
ZZ	zigzag instability
ζ	$c - \psi\theta$
θ	temperature deviation
ν	kinematic viscosity
ρ_0	mean density
Φ	velocity potential
τ	period of oscillations
Ψ	velocity potential
ω	frequency of oscillations